

Research articles

Force acting on a cluster of magnetic nanoparticles in a gradient field: A Langevin dynamics study

Andrey A. Kuznetsov

Institute of Continuous Media Mechanics UB RAS, Perm Federal Research Center UB RAS, 614013 Perm, Russia

ARTICLE INFO

Keywords:

Magnetophoresis
Magnetophoretic mobility
Magnetic nanoparticles
Magnetic beads
Langevin dynamics
Landau-Lifshitz-Gilbert equation

ABSTRACT

Magnetophoretic force acting on a rigid spherical cluster of single-domain nanoparticles in a constant-gradient weak magnetic field is investigated numerically using the Langevin dynamics simulation method. Nanoparticles are randomly and uniformly distributed within the cluster volume. They interact with each other via long-range dipole-dipole interactions. Simulations reveal that if the total amount of particles in the cluster is kept constant, the force decreases with increasing nanoparticle concentration due to the demagnetizing field arising inside the cluster. Numerically obtained force values with great accuracy can be described by the modified mean-field theory, which was previously successfully used for the description of various dipolar media. Within this theory, a new expression is derived, which relates the magnetophoretic mobility of the cluster with the concentration of nanoparticles and their dipolar coupling parameter. The expression shows that if the number of particles in the cluster is fixed, the mobility is a nonmonotonic function of the concentration. The optimal concentration values that maximize the mobility for a given amount of magnetic phase and a given dipolar coupling parameter are determined.

1. Introduction

Magnetic beads (or microspheres) are composite objects consisting of magnetic nanoparticles embedded in a spherical polymer matrix [1,2]. Nanoparticles can be homogeneously distributed within the bead volume, placed on its surface or concentrated in its center. Typical sizes of beads are 0.1–10 μm . The most promising applications of beads are in biotechnology and medicine. Among them are magnetic cell separation [3], targeted drug delivery [4] and single-molecule magnetic tweezers [5].

The physical basis for many applications of magnetic beads is the phenomenon of magnetophoresis, i.e. the motion of magnetic particles under the action of nonuniform magnetic field. It is known that the sensitivity of beads to the applied gradient field is among main factors determining their suitability for biomedical purposes [3]. As a result, there are many experimental studies on detailed magnetic characterization of different beads from different manufacturers [6–8]. The present work, on the contrary, uses a simplistic model of the magnetic bead to conduct a numerical and analytical study, which will hopefully provide new qualitative insights into how the magnetophoretic motion of the bead is affected by its size and magnetic content.

2. Model and methods

2.1. Problem formulation

The bead is modeled as a cluster of N identical spherical magnetic nanoparticles. The diameter d of particles is small enough (~ 10 nm) so that they can be considered as single-domain. Each particle has a magnetic moment \mathbf{m} , which can rotate freely inside the particle body and has a constant magnitude $m = \nu M_s$, where $\nu = (\pi/6)d^3$ is the particle volume, M_s is the saturation magnetization of the particle material. Particles are embedded in a rigid nonmagnetic spherical matrix of diameter D , their positions are fixed. The spatial distribution of particles is random and uniform, no overlapping is allowed. Dipole-dipole interactions between particles are taken into account. The cluster is placed in a nonmagnetic medium and subjected to a constant nonuniform magnetic field with a gradient G . For definiteness, an ideal quadrupole field is considered: $\mathbf{H} = (Gx, -Gy, 0)$ [9]. The schematic sketch of the investigated system is shown in Fig. 1. The primary task of this study is to determine the magnetic force \mathbf{F}_m acting on the cluster due to the field for a given \mathbf{R}_c , where $\mathbf{R}_c = (X_c, Y_c, Z_c)$ is the location of the cluster center.

Let us introduce a set of appropriate dimensionless parameters that determine the cluster behavior. The field magnitude can be characterized by the so-called Langevin parameter

E-mail address: kuznetsov.a@icmm.ru.<https://doi.org/10.1016/j.jmmm.2018.11.093>

Received 7 May 2018; Received in revised form 8 November 2018; Accepted 19 November 2018

Available online 19 November 2018

0304-8853/ © 2018 Elsevier B.V. All rights reserved.

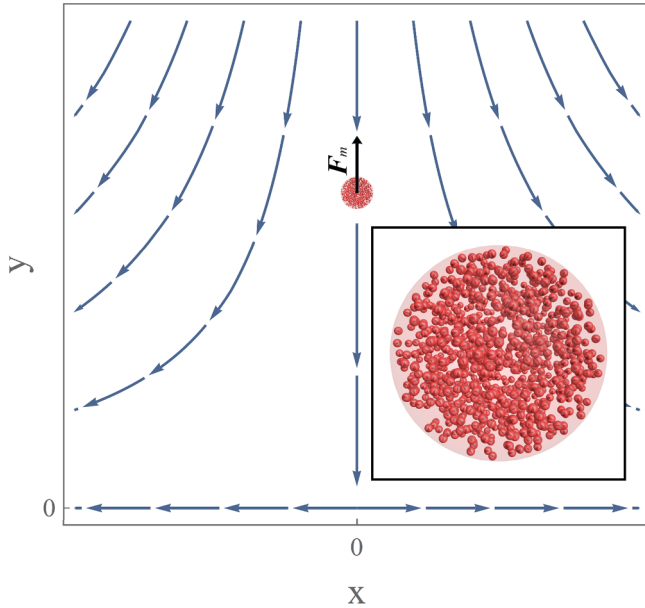


Fig. 1. Schematic sketch of the problem: field lines of the applied quadrupole field \mathbf{H} and the cluster positioned on the Y axis. The inset shows a snapshot of the cluster in its initial state when orientations of magnetic moments are random. The cluster parameters in the inset are $N = 1000$, $\varphi = 0.05$ and $D \approx 27d$.

$$\xi = \frac{\mu_0 m H}{k_B T}, \quad (1)$$

where μ_0 is the vacuum permeability, k_B is the Boltzmann constant, T is the system temperature. The Langevin parameter is the ratio between the magnetic (Zeeman) energy of a particle in the cluster and the thermal energy $k_B T$. The corresponding field vector is $\xi = g(x/d, -y/d, 0)$, where g is the dimensionless gradient parameter:

$$g = \frac{\mu_0 m G d}{k_B T}. \quad (2)$$

The intensity of intracluster dipole-dipole interactions can be characterized using the dipolar coupling parameter:

$$\lambda = \frac{\mu_0}{4\pi} \frac{m^2}{d^3 k_B T}. \quad (3)$$

It is known that the ground state of a pair of interacting magnetic particles is the “head-to-tail” configuration, when particles are in close contact and their magnetic moments are collinear [10]. The dipolar coupling parameter is the ratio between the interaction energy per particle in this state and the thermal energy of the system. Magnetite nanoparticles, which are typical in biomedical applications, can be used as an example to estimate these parameters. The saturation magnetization of bulk magnetite is $M_s \approx 450 \text{ kA} \cdot \text{m}^{-1}$ according to Ref. [11], but the value $M_s \approx 350 \text{ kA} \cdot \text{m}^{-1}$ is sometimes used for single-domain particles [12,13]. Thus, for magnetite nanoparticles with $d = 10 \text{ nm}$, the dipolar coupling parameter at temperature $T = 300 \text{ K}$ is $\lambda \approx 1$; for particles with 15 nm , it is $\lambda \approx 3\text{--}4.5$. Typical gradient values used in the so-called low gradient magnetic separation are $\mu_0 G \sim 10^2 \text{ T} \cdot \text{m}^{-1}$ [14]. For magnetite nanoparticles, this corresponds to $g \sim 10^{-4}$. Sometimes much larger gradients of the order of $\mu_0 G \sim 10^3 \text{ T} \cdot \text{m}^{-1}$ ($g \sim 10^{-3}$) are used [15]. As for the field magnitude itself, we will here mainly restrict ourselves to values $\xi \lesssim 1$. In this range, the magnetic response of a nanoparticle ensemble remains linear. For 10 nm magnetite particles, $\xi = 1$ corresponds to $H \approx 15 \text{ kA} \cdot \text{m}^{-1}$ (or to $B \approx 20 \text{ mT}$). This weak field range is relevant for many biomedical diagnostic systems [16–18]. Besides, this restriction on the field magnitude simplifies the simulation procedure, since now it is possible to neglect the magnetic anisotropy of real

single-domain particles. It is known that in the general case magnetic anisotropy can significantly effect the magnetization of uniaxial nanoparticles distributed in a solid matrix [19]. However, for noninteracting particles with the random easy-axis distribution, the initial slope of the magnetization curve does not depend on the anisotropy energy, it is always exactly the same as in the case of isotropic particles [20,21]. As for interacting uniaxial particles, our recent simulation study [22] also did not find any significant dependency between the weak-field magnetization and the anisotropy energy. The last important dimensionless parameter is the volume fraction (volume concentration) of nanoparticles inside the cluster:

$$\varphi = \frac{Nv}{V} = \frac{Nd^3}{D^3}, \quad (4)$$

where $V = (\pi/6)D^3$ is the cluster volume. The notation $x^* = x/d$ will be used for the reduced distance.

2.2. Langevin dynamics simulations

In order to accurately take into account the combined effect of the applied field, intracluster interactions and thermal fluctuations on the cluster behavior, the Langevin dynamics method is used. The Langevin equation that describes the magnetodynamics of a single-domain particle is the stochastic Landau-Lifshitz-Gilbert equation [23,24]. For the i th particle of the simulated cluster it reads

$$\frac{d\mathbf{m}_i}{dt} = -\gamma[\mathbf{m}_i \times \mathbf{H}_i^{\text{tot}}] - \frac{\gamma\alpha}{m}[\mathbf{m}_i \times [\mathbf{m}_i \times \mathbf{H}_i^{\text{tot}}]], \quad (5)$$

where $\gamma = \gamma_0/(1 + \alpha^2)$, γ_0 is the gyromagnetic ratio (measured in $\text{m} \cdot \text{A}^{-1} \cdot \text{s}^{-1}$), α is the phenomenological dimensionless damping constant, $\mathbf{H}_i^{\text{tot}} = \mathbf{H}_i^{\text{det}} + \mathbf{H}_i^{\text{fl}}$, $\mathbf{H}_i^{\text{det}}$ is the total deterministic field acting on the particle, it is the sum of the applied field and dipolar fields due to all other particles, \mathbf{H}_i^{fl} is the fluctuating thermal field. $\mathbf{H}_i^{\text{fl}}(t)$ is a Gaussian stochastic process with the following statistical properties:

$$\langle H_{i,k}^{\text{fl}}(t) \rangle = 0, \quad (6)$$

$$\langle H_{i,k}^{\text{fl}}(t_1) H_{j,l}^{\text{fl}}(t_2) \rangle = 2\mathcal{D}\delta_{ij}\delta_{kl}\delta(t_1 - t_2), \quad (7)$$

$$\mathcal{D} = \frac{\alpha k_B T}{\mu_0 m \gamma (1 + \alpha^2)}, \quad (8)$$

where k and l are Cartesian indices, angle brackets denote a mean value, δ_{ij} is the Kronecker delta, $\delta(t)$ is the Dirac delta function, \mathcal{D} is the strength of the thermal fluctuations. Eq. (5) can be rewritten in the dimensionless form:

$$\frac{d\mathbf{e}_i}{dt^*} = -\frac{1}{2\alpha}[\mathbf{e}_i \times \xi_i^{\text{tot}}] - \frac{1}{2}[\mathbf{e}_i \times [\mathbf{e}_i \times \xi_i^{\text{tot}}]], \quad (9)$$

where the $\mathbf{e}_i = \mathbf{m}_i/m$, $t^* = t/\tau_{\mathcal{D}}$ is the reduced time, $\tau_{\mathcal{D}} = \mu_0 m / 2\alpha\gamma k_B T$ is the characteristic time scale of the rotary diffusion of the magnetic moment (typically, $\tau_{\mathcal{D}} \sim 10^{-10} \text{ s}$ [13]), $\xi_i^{\text{tot}} = \mu_0 m \mathbf{H}_i^{\text{tot}} / k_B T = \xi_i^{\text{det}} + \xi_i^{\text{fl}}$,

$$\xi_i^{\text{det}} = \xi_i + \lambda \sum_{j \neq i}^N \left[\frac{3\mathbf{r}_{ij}^* (\mathbf{e}_j \cdot \mathbf{r}_{ij}^*)}{r_{ij}^{*5}} - \frac{\mathbf{e}_j}{r_{ij}^{*3}} \right], \quad (10)$$

$$\langle \xi_{i,k}^{\text{fl}}(t^*) \rangle = 0, \quad (11)$$

$$\langle \xi_{i,k}^{\text{fl}}(t_1^*) \xi_{j,l}^{\text{fl}}(t_2^*) \rangle = \frac{4\alpha^2}{1 + \alpha^2} \delta_{ij} \delta_{kl} \delta(t_1^* - t_2^*), \quad (12)$$

where $\xi_i = (g x_i^*, -g y_i^*, 0)$, $\mathbf{r}_{ij}^* = \mathbf{r}_i^* - \mathbf{r}_j^*$ is the vector between centers of particles i and j , $\mathbf{r}_i^* = (x_i^*, y_i^*, z_i^*)$.

The input parameters of the simulation are N , φ , λ , g and $\xi_c = \mu_0 m H_c / k_B T = g \sqrt{X_c^{*2} + Y_c^{*2}}$, where H_c is the value of the external field in the center of the cluster. In simulations, the cluster is always positioned on the Y axis: $X_c^* = Z_c^* = 0$, $Y_c^* > 0$. Using ξ_c , the cluster position is determined as $Y_c^* = \xi_c / g$. Using N and φ , the cluster diameter

is determined as $D^* = \sqrt[3]{N/\varphi}$. Then the cluster is generated as follows. The i th particle ($1 \leq i \leq N$) is randomly placed inside a cube with a side length of D and with the center located at $(0, Y_c, 0)$. If after this the particle is outside of the sphere of radius $D/2$ or if it overlaps with previously placed particles (i.e., with particles $j < i$), the position is rejected and the new position is generated. This is repeated until a suitable position is found. Then the initial state of \mathbf{e}_i is chosen at random. Then the state of the particle $i + 1$ is generated according to the same rules. After the cluster is generated, the standard Heun scheme [24] is used for numerical integration of Eqs. (9)–(12). The damping constant in simulations is $\alpha = 0.1$ and the integration time step is $\Delta t^* = 0.002$. After every time step, fields $\mathbf{g}_i^{\text{tot}}$ are recalculated using the current orientations of the particles. Dipolar interaction fields between every pair of particles in the cluster are calculated directly, without any truncations or approximations. Periodic boundary conditions are not used. Position and orientation of the cluster as a whole remain fixed during simulations. The following values of input parameters are investigated numerically: $0.25 \leq \xi \leq 2$, $1 \leq \lambda \leq 7$, $0.05 \leq \varphi \leq 0.45$, $g = 10^{-3}$, $N = 10^2$ – 10^3 .

The instantaneous force on a point-like magnetic moment due to external field is $\mu_0(\mathbf{m} \cdot \nabla)\mathbf{H}$ [25]. Then, for a quadrupole field, the force on the i th particle is

$$\mathbf{F}_{m,i} = \mu_0 m G (\mathbf{e}_{i,x}, -\mathbf{e}_{i,y}, 0). \quad (13)$$

If the field is large enough, the particle magnetic moment is always aligned with its direction and the magnitude of the force has its maximum value $\mu_0 m G$. For modeled systems the condition $gD^* \ll 1$ is typically fulfilled. It means that the field magnitude and direction do not significantly change within the cluster. In this case, all particles in the large field are also collinear with each other and the cluster is saturated, its total magnetic moment is $\mathcal{M}_{\text{sat}} = mN$ and the force is $F_{\text{sat}} = \mu_0 \mathcal{M}_{\text{sat}} G$. A normalized magnetic force then can be introduced as $\mathbf{f}_m = \mathbf{F}_m / F_{\text{sat}}$. For an arbitrary field magnitude, the net external force is calculated in simulations as

$$\mathbf{f}_m = \frac{\left\langle \sum_{i=1}^N \mathbf{F}_{m,i} \right\rangle}{F_{\text{sat}}} = \frac{1}{N} \left(\left\langle \sum_{i=1}^N \mathbf{e}_{i,x} \right\rangle, -\left\langle \sum_{i=1}^N \mathbf{e}_{i,y} \right\rangle, 0 \right). \quad (14)$$

To find this average quantity, the sampling of instantaneous force values starts after the time period of $t = 200\tau_{\mathcal{D}} \sim 10^{-8}$ – 10^{-7} s. In all considered cases, this time is enough for the simulated system to reach equilibrium. The total simulated period for each specific set of input parameters is about $2000\tau_{\mathcal{D}}$. Note that in biomedical applications, such as magnetic cell separation, typical velocities of magnetic microparticles are 10 – $10^2 \mu\text{m/s}$ [3]. So, the time it takes a microparticle to travel a distance equal to its diameter (10^{-3} – 10^{-1} s) is several orders of magnitude larger than the time required to achieve an equilibrium force value. This justifies the neglect of the cluster translational motion in simulations. The same reasoning remains valid even if magnetic anisotropy of particles is taken into account. It is known that anisotropy slows down the relaxation time of magnetic moments, but for 10 nm iron oxide particles this time is still comparable with $\tau_{\mathcal{D}}$ [11]. The situation can be more complicated for other magnetic materials. For example, 10 nm cobalt ferrite particles have the relaxation time $\gg 1$ s [26], so the cluster with such particles will presumably remain in a nonequilibrium state during its magnetophoretic motion. This situation is beyond the scope of the present work. For every particular set of input parameters, the force values are averaged not only over simulation time but also over ten independent realizations of the cluster. These realizations differ in positions of particles and initial orientations of magnetic moments. Such averaging can be also considered as an implicit account of the cluster rotation which may arise due to small inhomogeneities in the particle spatial distribution. In practice, force values for different realizations are very close. Error bars presented on the plots below show 95% confidence intervals for calculated averages.

2.3. Analytical solution

A much more common approach to the problem at hand is to consider the cluster as a homogeneous paramagnetic sphere of volume V . In this approximation, if the gradient is relatively small ($gD^* \ll 1$) and if the cluster and the surrounding medium are linearly magnetizable, the magnetic force on the cluster due to external field \mathbf{H} is [27,28]:

$$\mathbf{F}_m = \frac{3}{2} \mu_s \frac{\mu_c - \mu_s}{\mu_c + 2\mu_s} V \nabla H^2, \quad (15)$$

where μ_c and μ_s are absolute magnetic permeabilities of the cluster material and the surrounding medium, correspondingly. For the non-magnetic medium, $\mu_s = \mu_0$ and Eq. (15) reduces to

$$\mathbf{F}_m = \mu_0 \chi V \nabla (H^2/2), \quad (16)$$

$$\chi = \frac{\chi_c}{1 + \chi_c/3}, \quad (17)$$

where $\chi_c = \mu_c/\mu_0 - 1$ is the initial susceptibility of the cluster material. To elaborate on the meaning of the quantity χ , let us first consider an elongated cylindrical sample homogeneously filled with the magnetic material with the susceptibility χ_c . If a weak uniform magnetic field H is applied along the main axis of the cylinder, then the relation between the sample magnetization and the field is $M = \chi_c H$. For a spherical sample, the situation becomes more complicated. Now χ_c describes the relation between the magnetization and the magnetic field *inside* the sample H_{int} , i.e. $M = \chi_c H_{\text{int}}$. The internal field does not coincide with the applied one, the difference between two fields is called the demagnetizing field. It is created by the surface divergence of the sample's own magnetization [29]. For a sphere, the relation between applied and internal fields is $H = H_{\text{int}} + M/3$. It is easy to see, that for a sphere $M = \chi_c H / (1 + \chi_c/3) = \chi H$. So, χ can be considered as the cluster effective susceptibility. The total magnetic moment of the cluster is $\mathcal{M} = \chi V H$.

For a quadrupole field, the force Eq. (16) can be rewritten in the normalized form

$$\begin{aligned} \mathbf{f}_m &= \frac{\mu_0 \chi V G^2}{F_{\text{sat}}} (X_c, Y_c, 0) \\ &= \frac{\mu_0 \chi V G^2 \xi_c d}{F_{\text{sat}} g} \left(\frac{X_c^*}{\sqrt{X_c^{*2} + Y_c^{*2}}}, \frac{Y_c^*}{\sqrt{X_c^{*2} + Y_c^{*2}}}, 0 \right) \\ &= \frac{\chi_c^*}{3\chi_L} \left(\frac{X_c^*}{\sqrt{X_c^{*2} + Y_c^{*2}}}, \frac{Y_c^*}{\sqrt{X_c^{*2} + Y_c^{*2}}}, 0 \right), \end{aligned} \quad (18)$$

where χ_L is the so-called Langevin susceptibility, which describes the initial magnetic response of an ideal paramagnetic gas [20]:

$$\chi_L = \frac{\mu_0 m^2 N}{3k_B T V} = 8\lambda\varphi \quad (19)$$

Now the only unknown quantity is the initial susceptibility χ_c of the cluster material. In our case, this is a solid dispersion of interacting single-domain nanoparticles. To estimate χ_c , we will use the so-called modified mean-field theory (MMFT). This approach was first proposed for the description of static magnetic properties of concentrated ferrofluids [30,31]. MMFT also showed its effectiveness in the description of other media containing magnetic nanoparticles, such as ferrogels [32] and magnetic emulsions [33]. It was shown in Refs. [22,34] that MMFT is able to successfully describe the initial susceptibility of nanoparticles embedded in a solid nonmagnetic matrix. According to MMFT, the susceptibility of an ensemble of single-domain nanoparticles is given by

$$\chi_c = \chi_L (1 + \chi_L/3). \quad (20)$$

Then the cluster effective susceptibility takes the form

$$\chi = \chi_L \frac{1 + \chi_L/3}{1 + \chi_L/3 + \chi_L^2/9}. \quad (21)$$

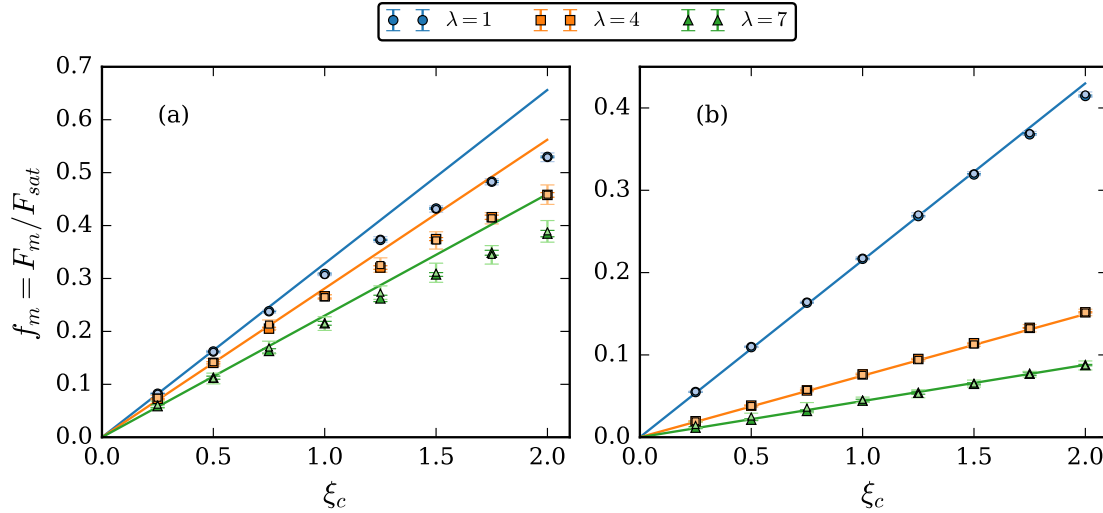


Fig. 2. Normalized magnetic force on the cluster vs. magnetic field in the center of the cluster. $\phi = 0.05$ (a) and 0.4 (b). Symbols are simulations results for $g = 0.001$. Different symbols correspond to different dipolar coupling parameters (see legend). Larger and darker symbols are for $N = 1000$, smaller and lighter symbols are for $N = 100$. Solid lines are analytical predictions from Eq. (24), for the same dipolar coupling parameters.

Eqs. (18) and (21) completely determine the magnetic force acting on the cluster. Their applicability range is to be tested via numerical simulations.

3. Results and discussion

3.1. Magnetic force

One the simulation results is that the force acting on the cluster positioned on the Y axis is directed predominantly along this axis, the average x -component of the force is zero within the error bar. Fig. 2 illustrates dependencies of the magnetic force magnitude on the magnetic field intensity ξ_c . It is seen that Eqs. (18) and (21) accurately describe simulation results in the weak field limit. With increasing field, the growth of the force slows down due to the fact that the cluster magnetization curve is nonlinear – its magnetic moment cannot be larger than \mathcal{M}_{sat} and the force cannot be larger than the corresponding value F_{sat} . It is noteworthy that the field range, where the linear response assumption is valid, increases with increasing particle concentration. In Fig. 2a, which corresponds to $\phi = 0.05$, nonlinearity becomes noticeable already at $\xi \simeq 1$, but in Fig. 2b ($\phi = 0.4$) the linear law Eq. (18) is valid up to $\xi = 2$. Fig. 2 gives simulation results for clusters of different sizes, $N = 100$ and $N = 1000$. Simulation points for two cases are very close and this is an encouraging result. Due to limited computational resources, we only investigate clusters with $N \sim 10^3$, which at the lowest considered concentrations $\phi \sim 0.1$ have a diameter of a few tenths of a micron. But the weak dependency of the cluster reduced properties on its size indicates that obtained results should remain relevant for larger structures with $D \sim 1\text{--}10\ \mu\text{m}$.

Simulations also show that the force acting on an N -particle cluster is smaller for more concentrated clusters. It is clearly seen in Fig. 3. In the limit $\phi \rightarrow 0$, the normalized force is $f_m = \xi_c/3$. With increasing ϕ , the force starts a nonlinear decline, which is more pronounced at larger coupling parameters λ . At $\lambda = 7$ and $\phi = 0.45$, the force drops by almost an order of magnitude. MMFT accurately describes simulation results for all considered values of ϕ and λ and can be used to analyze the observed behavior. The total magnetic moment of the cluster and the magnetic force Eq. (16) are proportional to the quantity $\chi V = (\chi/\phi)V_m$, where $V_m = vN$ is the total amount of magnetic material in the cluster. In the case when V is fixed, the force is controlled by the susceptibility χ , which is a measure of the magnetic response per unit volume. But if V_m is fixed (this is the case in simulations), the force is determined by χ/ϕ , which is a measure of the magnetic response per particle. If

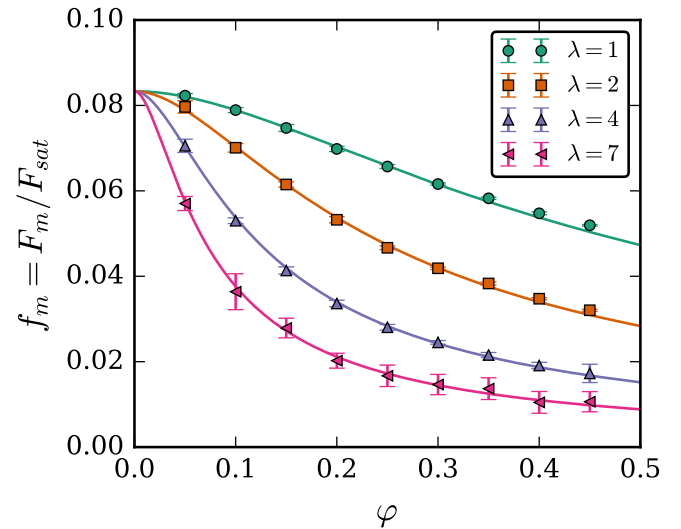


Fig. 3. Normalized magnetic force on the cluster vs. volume fraction of particles in the cluster. $\xi_c = 0.25$. Symbols are simulations results for $N = 500$ and $g = 0.001$. Different symbols correspond to different dipolar coupling parameters (see legend). Curves are analytical predictions from Eq. (24), for the same dipolar constants.

intracuster interactions between particles are neglected (the Langevin approximation), the susceptibility is given by the Langevin value $\chi = \chi_L$, which grows linearly with the concentration ϕ . As a result, for a given V_m , the quantity χ/ϕ and hence the force do not depend on the particle concentration. The force always equals to the zero-concentration value $F_m = (\xi_c/3)F_{sat} = (8\lambda V_m)\mu_0 GH_c$. Eq. (20) goes beyond the Langevin approximation and takes into account the fact that dipole–dipole interactions between an arbitrary particle and its local surroundings, on average, help the particle to align with the field. χ_c grows quadratically with the concentration and χ_c/ϕ grows linearly. Eq. (21) additionally takes into account the demagnetizing field, which is the long-range effect of dipole–dipole interactions. This field, in accordance with its name, weakens the response of an arbitrary particle to the applied field. The demagnetizing field is proportional to χ , which grows slower than linearly with ϕ and bounded from above by the value $\chi = 3$ (see Fig. 4 below). Consequently, at fixed V_m and large ϕ , the quantity χ/ϕ and hence the force decrease hyperbolically with the concentration, $F_m = (\xi_c/8\lambda\phi)F_{sat} = (3V_m/\phi)\mu_0 GH_c$.

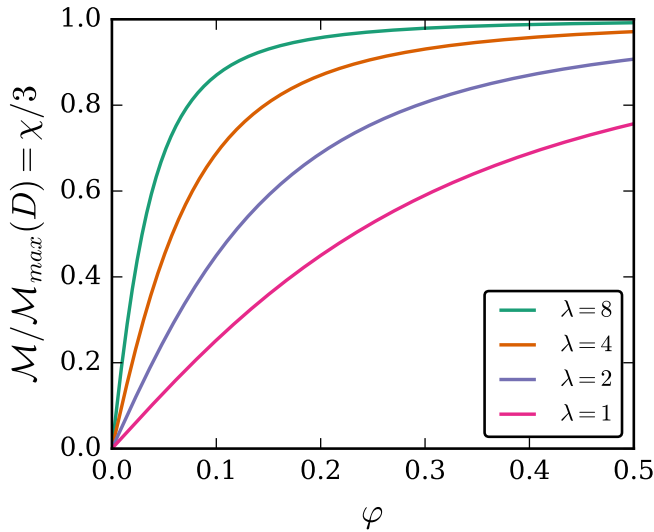


Fig. 4. Normalized magnetophoretic mobility of the cluster vs. volume fraction of particles in it [Eq. (24)]. The cluster diameter is fixed ($D = \text{const}$). Different curves correspond to different dipolar coupling parameters, from bottom to top: $\lambda = 1, 2, 4$ and 8 .

3.2. Magnetophoretic mobility

The analytical model based on MMFT shows very good agreement with the simulation results in a wide range of interaction parameters φ and λ . Potentially, the model can be used for an accurate description of the cluster magnetophoresis at temporal and spatial scales that are not easily accessible via direct nanoscale simulations. For example, the model can be used to obtain a universal expression for the so-called magnetophoretic mobility. It is known that magnetic microparticles moving in a viscous nonmagnetic liquid with time attain a constant velocity value u , which is determined by the balance between the magnetic force F_m and the drag force F_d [3]. The latter for spherical particles with low Reynolds numbers is given by the Stokes's law:

$$F_d = -3\pi\eta D u, \quad (22)$$

where η is the viscosity of the suspending liquid. In the general case, the drag force should contain the hydrodynamic diameter of the cluster D_h , which can be larger than D if the cluster core is covered by some nonmagnetic shell. But here we assume that two diameters coincide. From the balance condition $F_m = -F_d$ one obtains

$$u = \frac{\chi V}{3\pi\eta D} S_m, \quad (23)$$

where $S_m = \mu_0(\mathbf{H} \cdot \nabla)\mathbf{H} = \nabla(\mu_0 H^2/2)$ is known as the magnetophoretic driving force [3,8]. The proportionality factor $\mathcal{M} = \chi V/3\pi\eta D$ is the cluster magnetophoretic mobility. Using Eq. (21), the mobility can be rewritten as

$$\begin{aligned} \mathcal{M} &= \frac{\chi D^2}{18\eta} \\ &= \frac{\chi}{\varphi^{2/3}} \frac{1}{18\eta} \left[\frac{6}{\pi} V_m \right]^{2/3} \\ &= \frac{\chi_L^{1/3} (1 + \chi_L/3)}{1 + \chi_L/3 + \chi_L^2/9} \frac{4\lambda^{2/3}}{18\eta} \left[\frac{6}{\pi} V_m \right]^{2/3}. \end{aligned} \quad (24)$$

It should be emphasized that Eq. (24) is not specifically tied to a quadrupole field considered earlier. However, it still assumes that the field magnitude is small and the cluster response is linear. According to Eq. (24), the maximum possible mobility for a given diameter D is $\mathcal{M}_{\max}(D) = D^2/6\eta$. For $D = 1 \mu\text{m}$ and $\eta = 10^{-3} \text{ Pa}\cdot\text{s}$, this value is $\mathcal{M}_{\max} = 1.67 \cdot 10^{-10} \text{ m}^3(\text{T}\cdot\text{A}\cdot\text{s})^{-1}$. The concentration dependency of the normalized mobility $\mathcal{M}/\mathcal{M}_{\max}(D) = \chi/3$ simply repeats the concentration dependency of the susceptibility. Dependencies for different λ are

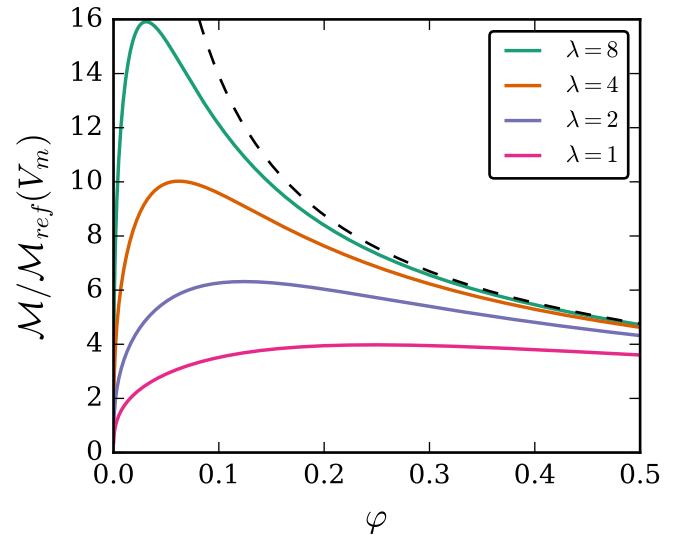


Fig. 5. Magnetophoretic mobility of the cluster vs. volume fraction of particles in it [Eq. (24)]. The total amount of magnetic phase in the cluster is fixed ($V_m = \text{const}$). Different solid curves correspond to different dipolar coupling parameters, from bottom to top: $\lambda = 1, 2, 4$ and 8 . Dashed line is the high-concentration asymptote $3/\varphi^{2/3}$.

shown in Fig. 4. Since the diameter is fixed, the friction coefficient $3\pi\eta D$ is constant and the increase in the concentration only leads to the slow increase in the magnetic force and hence in the mobility. A more complex concentration dependency is observed if, instead of D , the total amount of magnetic material V_m is fixed. The quantity $\mathcal{M}_{\text{ref}}(V_m) = (6V_m/\pi)^{2/3}/18\eta$ may be chosen as a reference mobility value for this case. For $N = 10^5$, $d = 10 \text{ nm}$ and $\eta = 10^{-3} \text{ Pa}\cdot\text{s}$, this value is $\mathcal{M}_{\text{ref}} = 1.2 \cdot 10^{-11} \text{ m}^3(\text{T}\cdot\text{A}\cdot\text{s})^{-1}$. Concentration dependencies of $\mathcal{M}/\mathcal{M}_{\text{ref}}(V_m)$ at different λ are given in Fig. 5. It is seen that dependencies are nonmonotonic, for every λ there is an optimal concentration value at which the mobility is maximal. The corresponding value of χ_L can be found by solving $(\partial \mathcal{M} / \partial \chi_L)_{\lambda, V_m} = 0$. It gives the optimal value of the Langevin susceptibility $\chi_{L, \text{opt}} \approx 1.9813$. Then the optimal volume fraction and diameter are

$$\varphi_{\text{opt}} = \frac{1.9813}{8\lambda}, \quad D_{\text{opt}} = \left[\frac{6}{\pi} \frac{V_m}{\varphi_{\text{opt}}} \right]^{1/3}. \quad (25)$$

The mobility under these optimal conditions is $\mathcal{M}_{\text{opt}} \approx 4\lambda^{2/3} \mathcal{M}_{\text{ref}}(V_m)$. The observed nonmonotonic dependency can be explained as follows. In the limit $\varphi \rightarrow 0$, the parameter $(\chi/\varphi)V_m$, which controls the magnetic force, has a definite finite value $8\lambda V_m$. On the contrary, the cluster diameter and hence the friction coefficient are infinitely large, so the mobility in this limit is zero. With increasing concentration, the friction coefficient decreases as $\sim 1/\varphi^{1/3}$ and the mobility initially increases as $\mathcal{M} = 8\lambda\varphi^{1/3} \mathcal{M}_{\text{ref}}(V_m)$. But at $\varphi > \varphi_{\text{opt}}$, the magnetic force decrease becomes hyperbolic (due to strong demagnetizing fields) and dominates over the drag decrease. As a result, the mobility eventually falls down as $\mathcal{M} = (3/\varphi^{2/3}) \mathcal{M}_{\text{ref}}(V_m)$.

4. Conclusions

In this work, the force acting on a polymer magnetic bead in a constant-gradient field is calculated by means of the Langevin dynamics method. The bead is modeled as a spherical rigid cluster of randomly distributed single-domain particles. The magnitude of the applied field is typically small enough so that the cluster magnetization remains a linear function of the field. It is demonstrated that if the total number of particles in the cluster is fixed, the increase in the particle concentration leads to the nonlinear decrease in the force magnitude. The reason for this is the demagnetizing field inside the cluster, which weakens the

response of an arbitrary particle to the applied field and hence decreases the cluster net average magnetic moment. It is also shown that the cluster can be successfully represented as a single paramagnetic particle whose magnetization obeys MMFT. The theory describes numerically obtained force values with great accuracy in a broad range of simulation parameters. Within MMFT, a new universal formula is obtained for the magnetophoretic mobility of an isolated cluster moving in a viscous nonmagnetic liquid. The formula shows that for a given number of particles and a given dipolar coupling parameter there is an optimal concentration value (and hence an optimal diameter) for which the mobility is maximal. Below this value, the mobility becomes smaller due to the increase of the cluster friction coefficient; above this value, the mobility becomes smaller due to the discussed decrease of the magnetic force.

In future, we hope to investigate a more general problem when nanoparticles do not occupy the whole bead, but instead distributed only in an outer spherical shell surrounding a nonmagnetic polymer core.

Acknowledgments

The work was supported by Russian Science Foundation (project No. 17-72-10033). Calculations were performed using the “URAN” supercomputer of IMM UB RAS.

References

- [1] A.Y. Gervald, I.A. Gritskova, N.I. Prokopov, Synthesis of magnetic polymeric microspheres, *Russ. Chem. Rev.* 79 (3) (2010) 219, <https://doi.org/10.1070/rc2010v079n03abeh004068>.
- [2] O. Philippova, A. Barabanova, V. Molchanov, A. Khokhlov, Magnetic polymer beads: recent trends and developments in synthetic design and applications, *Eur. Polym. J.* 47 (4) (2011) 542–559, <https://doi.org/10.1016/j.eurpolymj.2010.11.006>.
- [3] M. Zborowski, J.J. Chalmers, *Magnetic Cell Separation*, Elsevier, 2007.
- [4] S. Dutz, M.E. Hayden, A. Schaap, B. Stoeber, U.O. Häfeli, A microfluidic spiral for size-dependent fractionation of magnetic microspheres, *J. Magn. Magn. Mater.* 324 (22) (2012) 3791–3798, <https://doi.org/10.1016/j.jmmm.2012.06.014>.
- [5] M.M. van Oene, L.E. Dickinson, F. Pedaci, M. Köber, D. Dulin, J. Lipfert, N.H. Dekker, Biological magnetometry: torque on superparamagnetic beads in magnetic fields, *Phys. Rev. Lett.* 114 (21) (2015) 218301 <https://doi.org/10.1103/physrevlett.114.218301>.
- [6] J. Xu, K. Mahajan, W. Xue, J.O. Winter, M. Zborowski, J.J. Chalmers, Simultaneous, single particle, magnetization and size measurements of micron sized, magnetic particles, *J. Magn. Magn. Mater.* 324 (24) (2012) 4189–4199, <https://doi.org/10.1016/j.jmmm.2012.07.039>.
- [7] C. Zhou, E.D. Boland, P.W. Todd, T.R. Hanley, Magnetic particle characterization: magnetophoretic mobility and particle size, *Cytometry Part A* 89 (6) (2016) 585–593, <https://doi.org/10.1002/cyto.a.22866>.
- [8] D.T. Grob, N. Wise, O. Oduwale, S. Sheard, Magnetic susceptibility characterisation of superparamagnetic microspheres, *J. Magn. Magn. Mater.* 452 (2018) 134–140, <https://doi.org/10.1016/j.jmmm.2017.12.007>.
- [9] M. Zborowski, L. Sun, L.R. Moore, P.S. Williams, J.J. Chalmers, Continuous cell separation using novel magnetic quadrupole flow sorter, *J. Magn. Magn. Mater.* 194 (1–3) (1999) 224–230, [https://doi.org/10.1016/s0304-8853\(98\)00581-2](https://doi.org/10.1016/s0304-8853(98)00581-2).
- [10] I.S. Jacobs, C.P. Bean, An approach to elongated fine-particle magnets, *Phys. Rev.* 100 (4) (1955) 1060, <https://doi.org/10.1103/physrev.100.1060>.
- [11] R.E. Rosensweig, Heating magnetic fluid with alternating magnetic field, *J. Magn. Magn. Mater.* 252 (2002) 370–374, [https://doi.org/10.1016/S0304-8853\(02\)00706-0](https://doi.org/10.1016/S0304-8853(02)00706-0).
- [12] V. Schaller, G. Wahnström, A. Sanz-Velasco, S. Gustafsson, E. Olsson, P. Enoksson, C. Johansson, Effective magnetic moment of magnetic multicore nanoparticles, *Phys. Rev. B* 80 (9) (2009) 092406, <https://doi.org/10.1103/physrevb.80.092406>.
- [13] P. Ilg, Equilibrium magnetization and magnetization relaxation of multicore magnetic nanoparticles, *Phys. Rev. B* 95 (21) (2017) 214427 <https://doi.org/10.1103/physrevb.95.214427>.
- [14] S.S. Leong, S.P. Yeap, J. Lim, Working principle and application of magnetic separation for biomedical diagnostic at high- and low-field gradients, *Interface Focus* 6 (6) (2016) 20160048, <https://doi.org/10.1098/rsfs.2016.0048>.
- [15] J. Oberteuffer, High gradient magnetic separation, *IEEE Trans. Magn.* 9 (3) (1973) 303–306, <https://doi.org/10.1109/tmag.1973.1067673>.
- [16] N. Xia, T.P. Hunt, B.T. Mayers, E. Alsberg, G.M. Whitesides, R.M. Westervelt, D.E. Ingber, Combined microfluidic-micromagnetic separation of living cells in continuous flow, *Biomed. Microdevices* 8 (4) (2006) 299, <https://doi.org/10.1007/s10544-006-0033-0>.
- [17] D. Robert, N. Pamme, H. Conjeaud, F. Gazeau, A. Iles, C. Wilhelm, Cell sorting by endocytotic capacity in a microfluidic magnetophoresis device, *Lab. Chip* 11 (11) (2011) 1902–1910, <https://doi.org/10.1039/c0lc00656d>.
- [18] Y. Chen, Y. Xianyu, Y. Wang, X. Zhang, R. Cha, J. Sun, X. Jiang, One-step detection of pathogens and viruses: combining magnetic relaxation switching and magnetic separation, *ACS Nano* 9 (3) (2015) 3184–3191, <https://doi.org/10.1021/acsnano.5b00240>.
- [19] Y.L. Raikher, The magnetization curve of a textured ferrofluid, *J. Magn. Magn. Mater.* 39 (1–2) (1983) 11–13, [https://doi.org/10.1016/0304-8853\(83\)90385-2](https://doi.org/10.1016/0304-8853(83)90385-2).
- [20] C.P. Bean, J.D. Livingston, Superparamagnetism, *J. Appl. Phys.* 30 (4) (1959) S120–S129, <https://doi.org/10.1063/1.2185850>.
- [21] R.W. Chantrell, N.Y. Ayoub, J. Popplewell, The low field susceptibility of a textured superparamagnetic system, *J. Magn. Magn. Mater.* 53 (1–2) (1985) 199–207, [https://doi.org/10.1016/0304-8853\(85\)90150-7](https://doi.org/10.1016/0304-8853(85)90150-7).
- [22] A.A. Kuznetsov, Equilibrium magnetization of a quasispherical cluster of single-domain particles, *Phys. Rev. B* 98 (14) (2018) 144418 <https://doi.org/10.1103/PhysRevB.98.144418>.
- [23] W.F. Brown Jr., Thermal fluctuations of a single-domain particle, *Phys. Rev.* 130 (5) (1963) 1677, <https://doi.org/10.1103/PhysRev.130.1677>.
- [24] J.L. García-Palacios, F.J. Lázaro, Langevin-dynamics study of the dynamical properties of small magnetic particles, *Phys. Rev. B* 58 (22) (1998) 14937, <https://doi.org/10.1103/physrevb.58.14937>.
- [25] L.D. Landau, E.M. Lifshitz, *Electrodynamics of Continuous Media*, second ed., Pergamon, New York, 1984.
- [26] E.M. Claessens, B.H. Erne, I.A. Bakelaar, B.W.M. Kuipers, A.P. Philipse, Measurement of the zero-field magnetic dipole moment of magnetizable colloidal silica spheres, *J. Phys.: Condens. Matter* 19 (3) (2007) 036105 <https://doi.org/10.1088/0953-8984/19/3/036105>.
- [27] D.L. Cummings, D.A. Himmelmblau, J.A. Oberteuffer, G.J. Powers, Capture of small paramagnetic particles by magnetic forces from low speed fluid flows, *AIChE J.* 22 (3) (1976) 569–575, <https://doi.org/10.1002/aic.690220322>.
- [28] C. Rinaldi, An invariant general solution for the magnetic fields within and surrounding a small spherical particle in an imposed arbitrary magnetic field and the resulting magnetic force and couple, *Chem. Eng. Commun.* 197 (1) (2009) 92–111, <https://doi.org/10.1080/00986440903285621>.
- [29] R.I. Joseph, E. Schlömann, Demagnetizing field in nonellipsoidal bodies, *J. Appl. Phys.* 36 (5) (1965) 1579–1593, <https://doi.org/10.1063/1.1703091>.
- [30] A.F. Pshenichnikov, V.V. Mekhonoshin, A.V. Lebedev, Magneto-granulometric analysis of concentrated ferrocolloids, *J. Magn. Magn. Mater.* 161 (1996) 94–102, [https://doi.org/10.1016/s0304-8853\(96\)00067-4](https://doi.org/10.1016/s0304-8853(96)00067-4).
- [31] A.O. Ivanov, O.B. Kuznetsova, Magnetic properties of dense ferrofluids: an influence of interparticle correlations, *Phys. Rev. E* 64 (4) (2001) 041405 <https://doi.org/10.1103/physreve.64.041405>.
- [32] D.S. Wood, P.J. Camp, Modeling the properties of ferrogels in uniform magnetic fields, *Phys. Rev. E* 83 (1) (2011) 011402 <https://doi.org/10.1103/physreve.83.011402>.
- [33] A.O. Ivanov, O.B. Kuznetsova, Nonmonotonic field-dependent magnetic permeability of a paramagnetic ferrofluid emulsion, *Phys. Rev. E* 85 (4) (2012) 041405 <https://doi.org/10.1103/physreve.85.041405>.
- [34] A.F. Pshenichnikov, V.V. Mekhonoshin, Equilibrium magnetization and microstructure of the system of superparamagnetic interacting particles: numerical simulation, *J. Magn. Magn. Mater.* 213 (3) (2000) 357–369, [https://doi.org/10.1016/s0304-8853\(99\)00829-x](https://doi.org/10.1016/s0304-8853(99)00829-x).